JOURNAL OF GUIDANCE, CONTROL, AND DYNAMICS
Vol. 29, No. 1, January–February 2006

Formation Design in Eccentric Orbits Using Linearized Equations of Relative Motion

Christopher Lane* and Penina Axelrad†
University of Colorado, Boulder, Colorado 80309-0431

Geometrical methods for formation flying design based on the analytical solution to Hill's equations have been previously developed and used to specify desired relative motions in near circular orbits. These approaches offer valuable insight into the relative motion and allow for the rapid design of satellite configurations to achieve mission specific requirements, such as vehicle separation at perigee or apogee, minimum separation, or a particular geometrical shape. A comparable set of geometrical relationships for formations in eccentric orbits, where Hill's equations are not valid, is presented. The use of these relationships to investigate formation designs and their evolution in time is demonstrated.

Nomenclature

A	=	amplitude parameter
a	=	semimajor axis
$\boldsymbol{C}$	=	unit vector in cross-track directon
E	=	eccentric anomaly
e	=	eccentricity
$\boldsymbol{I}$	=	unit vector in in-track direction
i	=	inclination
M	=	mean anomaly
n	=	mean motion
P	=	magnitude of position error
$\boldsymbol{R}$	=	unit vector in radial direction
r	=	magnitude of $\boldsymbol{r}$
$\boldsymbol{r}$	=	Earth-centered-inertial (ECI) position vector
S	=	sensitivity matrix
T	=	transformation matrix from ECI coordinates to RIC coordinates
t	=	time
V	=	magnitude of velocity error
$\boldsymbol{v}$	=	ECI velocity vector
W_e	=	rotation rate of Earth, $7.2921158553 \times 10^{-5}$ rad/s
x	=	radial position distance from origin of radial, in-track, cross-track (RIC) frame
y	=	in-track position distance from origin of RIC frame
z	=	cross-track position distance from origin of RIC frame
α	=	generic orbital element, for example, a, e, i, Ω, ω, or M_0
γ	=	phase angle in in-track/cross-track plane
$\Delta\alpha$	=	small perturbation in α
θ	=	argument of latitude
μ	=	gravitational parameter of Earth, $3.986004418 \times 10^{14}$ m^3/s^2
ν	=	true anomaly
ξ	=	cross-track angular separation
ρ	=	distance between two points in RIC frame
φ	=	in-track angular separation
ψ	=	phase parameter
Ω	=	right ascension of ascending node
ω	=	argument of perigee

Subscripts

a	=	value at apogee
ECI	=	ECI frame
FF	=	follower formation
ICF	=	in-track/cross-track formation
IF	=	in-track formation
pert	=	perturbed orbit
RIC	=	RIC frame
0	=	value at perigee
2body	=	two-body orbit

Received 1 September 2004; revision received 17 December 2004; accepted for publication 20 December 2004.

*Graduate Student, Aerospace Engineering Sciences, 431 UCB; christopher.lane@colorado.edu. Student Member AIAA.

†Associate Professor, Aerospace Engineering Sciences, 431 UCB; penina.axelrad@colorado.edu. Associate Fellow AIAA.

I. Introduction

FORMATION flying has received much attention in recent years because of the possible advantages of replacing a single, complex vehicle with a cluster of smaller, simpler ones. Flying a formation of vehicles offers improved flexibility and redundancy and the ability to construct much larger virtual sensors than can be flown on a single, monolithic vehicle. Many proposed missions, by both NASA and ESA, have identified formation flying as an enabling technology for increasing the science return while simultaneously decreasing the total mission risk. Examples include the Space Technology 5 mission,[1] Stellar Imager,[2] Terrestrial Planet Finder,[3] the Magnetospheric Multiscale Mission,[4] and Darwin.[5]

The development of relative motion equations for vehicles in eccentric orbits is well documented in the literature primarily to investigate the problem of rendezvous. Lawden[6] first presented a solution for the relative motion of two vehicles in nearby eccentric orbits in 1954, although the equations contain a singularity when the true anomaly of the reference orbit is a multiple of 180 deg. A key feature of this solution is the mapping of the differential equations governing the relative motion from the time domain to the true anomaly domain.

Tschauner and Hempel[7] presented a similar set of equations that also use true anomaly as the independent variable, but avoid the singularity in Ref. 6 by confining the results to eccentric orbits. Carter[8] later extended Lawden's[6] solution by removing the singularity. Note that all of these authors used an algebraic approach to find relative motion solutions. Garrison et al.[9] obtained a somewhat more intuitive result by using a geometric approach that referenced small position and velocity differences to small differences in the classical orbital elements of the vehicles. Gim and Alfriend[10] used a similar method, with a more robust set of orbital elements, to account for the perturbation due to J_2, although the resulting equations are in the form of a series expansion in eccentricity. The solutions obtained in Refs. 9 and 10 are functions of the true anomaly difference between the vehicles, which varies nonuniformly with time. This dependence shows up as a direct result of the use of true anomaly as the independent variable. Sabol et al.[11] derived a solution similar

to that of Garrison et al.,[9] but incorporated a Fourier–Bessel expansion of the true anomaly in terms of the mean anomaly and eccentricity. The expansion is cumbersome, particularly for high eccentricity cases. Relative motion equations derived by Melton[12] are completely explicit in time, but are also in the form of a series expansion in eccentricity.

Previous geometrical methods for formation design, such as the methods developed by Sabol et al.[13] and Lovell and Tragresser,[14] have focused on the analytical solution to Hill's equation,[15] which restricts their applicability to near-circular reference orbits. Obviously these methods are not well suited for formation design in eccentric orbits. Inalhan et al.[16] use the results obtained by Lawden[6] and Carter[8] to develop an initialization procedure for formations in eccentric orbits. The procedure, however, is involved, requiring the evaluation of a definite integral and the use of the monodromy matrix,[16] to obtain conditions for periodic formation geometries.

This paper focuses on formation design for unperturbed, eccentric orbits using a simple geometrical approach. The design method is derived from relative motion equations similar to those presented by Broucke.[17] This approach is attractive for two reasons. First, the solution is formulated with time as the independent variable, meaning the differential equations governing the relative motion are not mapped to true anomaly. More important, the equations are expressed as simple functions of a constant set of orbital element differences, and therefore, a great deal of insight can be gained from them.

The remainder of this paper develops a set of geometrical relationships for formations in eccentric orbits and shows how they can be used for formation design. These expressions permit the use of intuitive design methods, similar to the methods discussed in Refs. 13 and 14 for circular orbits, to be used to specify formation parameters in eccentric orbits. The validity and accuracy of the proposed design method, both for ideal two-body orbits and in the presence of perturbations, are shown in several examples.

II. Linearized Equations of Relative Motion in Elliptic Orbits

This section presents the derivation of a set of geometrical relationships describing the relative motion of two vehicles in nearby eccentric orbits. The primary vehicle, termed the chief, follows an unperturbed, eccentric trajectory that is referred to as the reference orbit. (Note that quantities without subscripts refer to the chief unless otherwise noted in the Nomenclature.) The reference orbit is completely described by the set of orbital elements $\alpha = [a, e, i, \Omega, \omega, M_0]^T$. The secondary vehicle, termed the deputy, is in a similar orbit with only a small change in orbital elements: $\alpha_{\text{deputy}} = \alpha + \Delta\alpha$. The derivation requires the assumption that the orbital elements of the chief and deputy are similar, that is, $\Delta\alpha \ll \alpha$; no assumptions about the eccentricity of the reference orbit are made.

The development begins by finding the sensitivity of the reference orbit to changes in α. The Earth-centered-inertial (ECI) position and velocity vectors of the chief are related to α through the following expressions[18]:

$$\boldsymbol{r} = r \begin{bmatrix} \cos(\Omega)\cos(\theta) - \sin(\Omega)\cos(i)\sin(\theta) \\ \sin(\Omega)\cos(\theta) + \cos(\Omega)\cos(i)\sin(\theta) \\ \sin(i)\sin(\theta) \end{bmatrix} \tag{1}$$

$$\boldsymbol{v} = \sqrt{\frac{\mu}{a(1-e^2)}} \begin{Bmatrix} -\cos(\Omega)[\sin(\theta) + e\sin(\omega)] - \sin(\Omega)\cos(i)[\cos(\theta) + e\cos(\omega)] \\ -\sin(\Omega)[\sin(\theta) + e\sin(\omega)] + \cos(\Omega)\cos(i)[\cos(\theta) + e\cos(\omega)] \\ \sin(i)[\cos(\theta) + e\cos(\omega)] \end{Bmatrix} \tag{2}$$

where

$$r = \frac{a(1-e^2)}{1 + e\cos(\nu)} \tag{3}$$

The sensitivity matrix S_{ECI} is constructed by assembling the partials of each component of $\boldsymbol{r}$ with respect to each orbital element in α. The details are given in the Appendix.

A natural coordinate frame for describing the relative motion of the deputy about the chief is the radial, in-track, cross-track (RIC) frame shown in Fig. 1. This is a noninertial frame that moves with the chief. Evaluated at the chief, the fundamental directions of this frame are

$$\boldsymbol{R} = \frac{\boldsymbol{r}}{r}, \qquad \frac{\mathrm{d}\boldsymbol{R}}{\mathrm{d}t} = \frac{\boldsymbol{v}}{r} - \frac{\boldsymbol{r}\cdot\boldsymbol{v}}{r^3}\boldsymbol{r}, \qquad \boldsymbol{C} = \frac{\boldsymbol{r}\times\boldsymbol{v}}{|\boldsymbol{r}\times\boldsymbol{v}|}, \qquad \frac{\mathrm{d}\boldsymbol{C}}{\mathrm{d}t} = 0$$

$$\boldsymbol{I} = \boldsymbol{C}\times\boldsymbol{R}, \qquad \frac{\mathrm{d}\boldsymbol{I}}{\mathrm{d}t} = \boldsymbol{C}\times\frac{\mathrm{d}\boldsymbol{R}}{\mathrm{d}t} \tag{4}$$

Thus, at the chief, the transformation matrix T relating the ECI frame to the RIC frame is given by[19]

$$T = \begin{bmatrix} \cos(\Omega)\cos(\theta) - \sin(\Omega)\cos(i)\sin(\theta) & \sin(\Omega)\cos(\theta) + \cos(\Omega)\cos(i)\sin(\theta) & \sin(i)\sin(\theta) \\ -\cos(\Omega)\sin(\theta) - \sin(\Omega)\cos(i)\cos(\theta) & -\sin(\Omega)\sin(\theta) + \cos(\Omega)\cos(i)\cos(\theta) & \sin(i)\cos(\theta) \\ \sin(\Omega)\sin(i) & -\cos(\Omega)\sin(i) & \cos(i) \end{bmatrix} \tag{5}$$

The partials of $\boldsymbol{r}$ with respect to α can be expressed in RIC by premultiplying S_{ECI} (Appendix) by T. This results in the RIC sensitivity matrix S_{RIC},

$$S_{\text{RIC}} = T S_{\text{ECI}} = \begin{bmatrix} \dfrac{r}{a} - \dfrac{3n(t-t_0)e\sin(\nu)}{2\sqrt{1-e^2}} & -a\cos(\nu) & 0 & 0 & 0 & \dfrac{ae\sin(\nu)}{\sqrt{1-e^2}} \\ -\dfrac{3an(t-t_0)\sqrt{1-e^2}}{2r} & \left(a + \dfrac{r}{1-e^2}\right)\sin(\nu) & 0 & r\cos(i) & r & \dfrac{a^2}{r}\sqrt{1-e^2} \\ 0 & 0 & r\sin(\theta) & -r\sin(i)\cos(\theta) & 0 & 0 \end{bmatrix} \tag{6}$$

Thus, S_{RIC} is a mapping relating orbital element differences between the chief and deputy (the column space of S) to radial, in-track, and cross-track position differences (the row space of S).

Figure 1 shows the set of curvilinear coordinates used to represent the relative position of the deputy with respect to the chief. At the chief, these coordinates are aligned with the unit vectors given in Eq. (4). In Fig. 1, a reference sphere of radius r is defined, tangent to the $\boldsymbol{I}$–$\boldsymbol{C}$ plane at the chief. The radial component of the relative position x is the difference between r_{deputy} and r; the curvilinear in-track and cross-track relative positions, y and z, are measured along the surface of the reference sphere as indicated in Fig. 1.

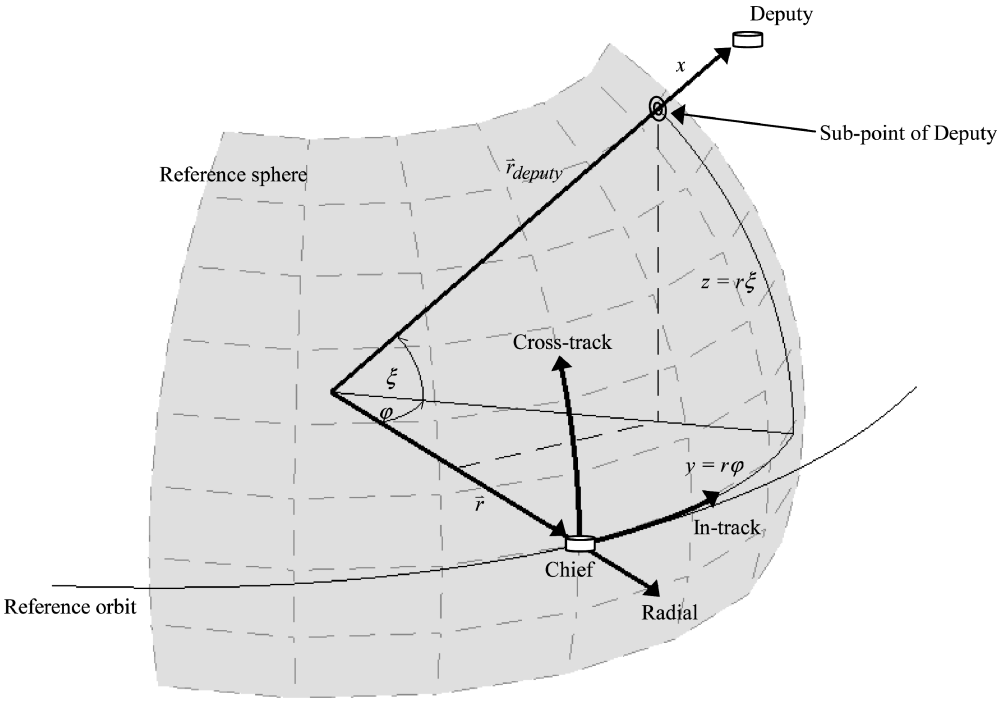

Fig. 1 RIC frame.

Mathematically they are defined as follows. The radial component x is given by

$$x = r_{\text{deputy}} - r, \qquad \dot{x} = (\boldsymbol{r}_{\text{deputy}} \cdot \boldsymbol{v}_{\text{deputy}})/r_{\text{deputy}} - (\boldsymbol{r} \cdot \boldsymbol{v})/r \tag{7}$$

The in-track component y is given by

$$y = r\varphi, \qquad \dot{y} = [(\boldsymbol{r} \cdot \boldsymbol{v})/r]\varphi + r\dot{\varphi} \tag{8}$$

where

$$\varphi = \sin^{-1}(\boldsymbol{R}_{\text{deputy}} \cdot \boldsymbol{I}), \qquad \dot{\varphi} = \frac{1}{\cos(\varphi)}\left(\boldsymbol{R}_{\text{deputy}} \cdot \frac{\mathrm{d}\boldsymbol{I}}{\mathrm{d}t} + \frac{\mathrm{d}\boldsymbol{R}_{\text{deputy}}}{\mathrm{d}t} \cdot \boldsymbol{I}\right)$$

$$\boldsymbol{R}_{\text{deputy}} = \frac{\boldsymbol{r}_{\text{deputy}}}{r_{\text{deputy}}}, \qquad \frac{\mathrm{d}\boldsymbol{R}_{\text{deputy}}}{\mathrm{d}t} = \frac{\boldsymbol{v}_{\text{deputy}}}{r_{\text{deputy}}} - \frac{\boldsymbol{r}_{\text{deputy}} \cdot \boldsymbol{v}_{\text{deputy}}}{r^3_{\text{deputy}}}\boldsymbol{r}_{\text{deputy}}$$

The cross-track component z is given by

$$z = r\xi, \qquad \dot{z} = [(\boldsymbol{r} \cdot \boldsymbol{v})/r]\xi + r\dot{\xi} \tag{9}$$

where

$$\xi = \sin^{-1}(\boldsymbol{R}_{\text{deputy}} \cdot \boldsymbol{C}), \qquad \dot{\xi} = \frac{1}{\cos(\xi)}\left(\frac{\mathrm{d}\boldsymbol{R}_{\text{deputy}}}{\mathrm{d}t} \cdot \boldsymbol{C}\right)$$

Thus, given the ECI position and velocity vectors of the chief and deputy, Eqs. (7–9) can be used to compute the curvilinear representation of the relative position of the deputy with respect to the chief.

Evaluated at the chief, the sensitivity of the curvilinear coordinates x, y, and z to orbit element differences is equal to S_{RIC} given in Eq. (6). Thus, for small orbital element differences, the resulting x, y, and z coordinates of the deputy are computed by $S_{\text{RIC}}\Delta\alpha$. This yields

$$x = \left[\frac{r}{a} - \frac{3n(t-t_0)e\sin(\nu)}{2\sqrt{1-e^2}}\right]\Delta a - a\cos(\nu)\Delta e + \frac{ae\sin(\nu)}{\sqrt{1-e^2}}\Delta M$$

$$y = \left[-\frac{3an(t-t_0)\sqrt{1-e^2}}{2r}\right]\Delta a + \left(a + \frac{r}{1-e^2}\right)\sin(\nu)\Delta e + \frac{a^2}{r}\sqrt{1-e^2}\Delta M + r[\Delta\omega + \cos(i)\Delta\Omega]$$

$$z = r\sin(\theta)\Delta i - r\sin(i)\cos(\theta)\Delta\Omega \tag{10}$$

The velocity equations are obtained by taking the time derivatives of Eq. (10),

$$\dot{x} = \frac{\mathrm{d}x}{\mathrm{d}t} = -\left[\frac{ne\sin(\nu)}{2\sqrt{1-e^2}} + \frac{3a^2}{r^2}n^2(t-t_0)e\cos(\nu)\right]\Delta a + n\sin(\nu)\sqrt{1-e^2}\left(\frac{a^3}{r^2}\right)\Delta e + en\cos(\nu)\left(\frac{a^3}{r^2}\right)\Delta M$$

$$\dot{y} = \frac{\mathrm{d}y}{\mathrm{d}t} = \left[\frac{3a^2}{2r^2}n^2(t-t_0)e\sin(\nu) - \frac{3a}{2r}n\sqrt{1-e^2}\right]\Delta a + \left[n\sqrt{1-e^2}\left(1+\frac{r}{p}\right)\left(\frac{a^3}{r^2}\right)\cos(\nu) + \frac{aen\sin^2(\nu)}{(1-e^2)^{\frac{3}{2}}}\right]\Delta e - en\sin(\nu)\left(\frac{a^3}{r^2}\right)\Delta M + \frac{aen\sin(\nu)}{\sqrt{1-e^2}}\Delta\omega + \frac{aen\cos(i)\sin(\nu)}{\sqrt{1-e^2}}\Delta\Omega$$

$$\dot{z} = \frac{\mathrm{d}z}{\mathrm{d}t} = \frac{an}{\sqrt{1-e^2}}\{\sin(i)[\sin(\theta) + e\sin(\omega)]\Delta\Omega + [\cos(\theta) + e\cos(\omega)]\Delta i\} \tag{11}$$

The expressions for the coplanar motion of the deputy (x, y, $\dot{x}$, $\dot{y}$) are similar to those developed in Ref. 17, but the expressions for y and $\dot{y}$ in Ref. 17 do not include a dependence on $\Delta\Omega$ because Broucke[17] only considered coplanar motion of the deputy. To understand what causes the in-track dependence on $\Delta\Omega$, consider the case when the ascending nodes of the chief and deputy orbit differ, as shown in Fig. 2. In this case, the argument of perigee of the chief and deputy are measured in slightly different planes; this causes an in-track offset of the deputy.

III. Geometry of Relative Motion in Elliptical Reference Orbit

Based on Eq. (10), geometrical relationships that describe the relative motion in an eccentric orbit are established. Stable formations with no drift are of primary interest, and thus, the secular growth

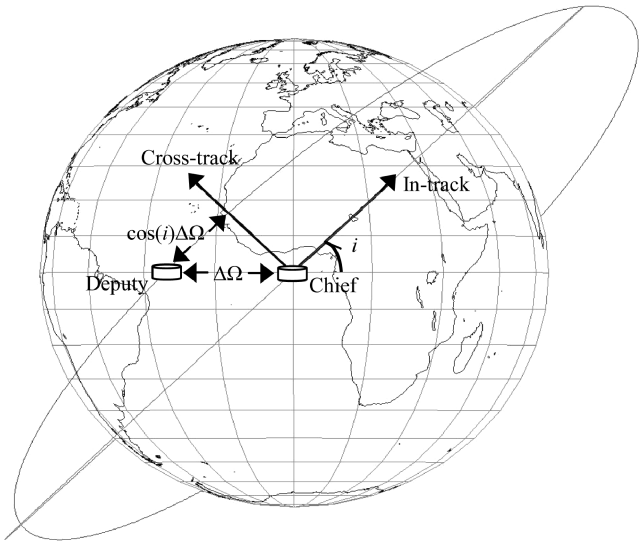

Fig. 2 Effect of nodal difference on in-track position.

in the separation between the vehicles is eliminated by constraining the energy of the orbits to be equal, that is, $\Delta a = 0$. This leaves

$$x = -a\cos(\nu)\Delta e + \frac{ae\sin(\nu)}{\sqrt{1-e^2}}\Delta M$$

$$y = \left(a + \frac{r}{1-e^2}\right)\sin(\nu)\Delta e + \frac{a^2}{r}\sqrt{1-e^2}\Delta M + r[\Delta\omega + \cos(i)\Delta\Omega]$$

$$z = r\sin(\theta)\Delta i - r\sin(i)\cos(\theta)\Delta\Omega \tag{12}$$

Other approaches for constraining the secular growth between the vehicles are needed when perturbations cause additional secular drifts.[20] However, in unperturbed orbits, setting $\Delta a = 0$ is sufficient.

Note that all of the terms in Eq. (12) have an implicit dependence on time through r, ν, and θ. With some algebraic manipulation, Eq. (12) can be written as

$$x = A_1\sin(\nu - \psi_1)$$

$$y = A_1\cos(\nu - \psi_1) - A_2\cos(E + \psi_2) + c_1$$

$$z = A_3\sin(E + \psi_3) - c_2 \tag{13}$$

where the eccentric anomaly and the constants are defined as

$$\sin(E) = \frac{\sin(\nu)\sqrt{1-e^2}}{1 + e\cos(\nu)}, \qquad \cos(E) = \frac{e + \cos(\nu)}{1 + e\cos(\nu)} \tag{14}$$

$$A_1 \equiv a\sqrt{\Delta e^2 + \frac{e^2\Delta M^2}{1-e^2}}$$

$$A_2 \equiv a\sqrt{\frac{\Delta e^2}{1-e^2} + e^2[\cos(i)\Delta\Omega + \Delta\omega]^2}$$

$$A_3 \equiv a\sqrt{\beta_1^2 + \beta_2^2} \tag{15}$$

$$\beta_1 = \sin(\omega)\Delta i - \sin(i)\cos(\omega)\Delta\Omega$$

$$\beta_2 = \sqrt{1-e^2}[\cos(\omega)\Delta i + \sin(i)\sin(\omega)\Delta\Omega] \tag{16}$$

$$c_1 = a\left[\frac{\Delta M}{\sqrt{1-e^2}} + \cos(i)\Delta\Omega + \Delta\omega\right], \qquad c_2 = ae\beta_1 \tag{17}$$

$$\sin(\psi_1) = \frac{a\Delta e}{A_1}, \qquad \cos(\psi_1) = \frac{ae\Delta M}{A_1\sqrt{1-e^2}} \tag{18}$$

$$\sin(\psi_2) = \frac{a\Delta e}{A_2\sqrt{1-e^2}}$$

$$\cos(\psi_2) = \frac{ae[\cos(i)\Delta\Omega + \Delta\omega]}{A_2} \tag{19}$$

$$\sin(\psi_3) = \frac{a\beta_1}{A_3}, \qquad \cos(\psi_3) = \frac{a\beta_2}{A_3} \tag{20}$$

The geometrical structure of Eq. (13) can be used to investigate formation designs and how they evolve with time.

IV. Formation Design

Inspection of Eq. (13) reveals that, in general, the relative motion in an eccentric reference orbit will not be an ellipse in any plane. This is a significant departure (and complication) from the analytical solution to Hill's equations,[15] in which the motion in the radial/in-track plane is always a 2×1 ellipse with the major axis in the in-track direction. Elliptical motion is possible in both the in-track/cross-track and radial/in-track planes, but only when certain conditions are imposed on the motion. The nonelliptical motion is due to the eccentricity of the reference orbit. In an eccentric reference orbit, $E \neq \nu$, except at perigee and apogee, and thus, the terms that vary with the eccentric anomaly have a different time dependence than those that vary with the true anomaly.

Five design parameters may be specified in Eq. (13). Three of the parameters, Δe, $\Delta\omega$, and ΔM, only affect the radial/in-track motion, and Δi only affects the out-of-plane motion, that is, cross-track motion. Both types of motion are affected by $\Delta\Omega$.

In the following sections, three types of formations are examined: 1) an in-track formation, 2) a follower formation, and 3) an in-track/cross-track formation. For each formation, the orbital element differences needed to establish the formation at perigee are derived.

A. In-Track Formations

Purely in-track motion is achieved by requiring the radial and cross-track positions of the deputy to always be zero. Thus, A_1, A_3, and c_2 must be zero in Eq. (13). This is achieved by setting $\Delta e_{\mathrm{IF}} = \Delta M_{\mathrm{IF}} = \Delta i_{\mathrm{IF}} = \Delta\Omega_{\mathrm{IF}} = 0$. Note that $\Delta e = 0$ implies that $\psi_2 = 0$ in Eq. (19) and, thus, Eq. (13) collapses to

$$x_{\mathrm{IF}} = 0, \qquad y_{\mathrm{IF}} = r\Delta\omega_{\mathrm{IF}}, \qquad z_{\mathrm{IF}} = 0 \tag{21}$$

The remaining design parameter in Eq. (21) is $\Delta\omega_{\mathrm{IF}}$, which represents a desired in-track separation at a particular time in the orbit. A separation of ρ_0 at perigee is created by setting

$$\Delta\omega_{\mathrm{IF}} = \rho_0/a(1-e) \tag{22}$$

The minimum and maximum separation between the chief and deputy in an in-track formation is derived from inspection of Eq. (21). The minimum separation occurs at perigee and is equal to

$$\rho_{\mathrm{IF}_{\min}} = a\Delta\omega_{\mathrm{IF}}(1-e) \tag{23}$$

The maximum separation occurs at apogee and is equal to

$$\rho_{\mathrm{IF}_{\max}} = a\Delta\omega_{\mathrm{IF}}(1+e) \tag{24}$$

B. Follower Formations

A follower formation is one in which the vehicles share the same groundtrack. For two vehicles to trace the same groundtrack they must pass over the same set of points on the Earth. This is accomplished by offsetting the nodal separation $\Delta\Omega$ to account for ΔM and the rotation rate of the Earth W_e. In particular,

$$\Delta\Omega_{\mathrm{FF}} = -(W_e/n)\Delta M_{\mathrm{FF}} \tag{25}$$

as derived in Sabol et al.[13] Note that Eq. (25) is only applicable when $\Delta a = 0$. If $\Delta a \neq 0$, then n for each vehicle is different, and Eq. (25) is no longer valid.

All vehicles in a follower formation must have the same eccentricity, inclination, and argument of perigee. (Vallado[19] provides a detailed discussion of groundtracks.) Thus, $\Delta e_{FF} = \Delta i_{FF} = \Delta\omega_{FF} = 0$, and Eq. (13) reduces to

$$x_{FF} = \frac{ae\sin(\nu)}{\sqrt{1-e^2}}\Delta M_{FF}$$

$$y_{FF} = \frac{a^2}{r}\sqrt{1-e^2}\Delta M_{FF} + r\cos(i)\Delta\Omega_{FF}$$

$$z_{FF} = -r\sin(i)\cos(\theta)\Delta\Omega_{FF} \tag{26}$$

When Eq. (26) is used, the separation between the chief and deputy at perigee is

$$\rho_0 = \sqrt{x_{FF_0}^2 + y_{FF_0}^2 + z_{FF_0}^2} = a\Big\{[(1+e)/(1-e)]\Delta M_{FF}^2 + (1-e)^2[\cos^2(i) + \sin^2(i)\cos^2(\omega)]\Delta\Omega_{FF}^2 + 2\sqrt{1-e^2}\cos(i)\Delta M_{FF}\Delta\Omega_{FF}\Big\}^{\frac{1}{2}} \tag{27}$$

Notice Eqs. (25) and (27) are a set of linearly independent algebraic equations that can be solved simultaneously for ΔM_{FF} and $\Delta\Omega_{FF}$. This yields

$$\Delta M_{FF} = \pm\frac{\rho_0}{a}\left\{\frac{1+e}{1-e} - 2\frac{W_e\cos(i)\sqrt{1-e^2}}{n} + \frac{W_e^2(1-e)^2}{n^2}[\cos^2(i) + \sin^2(i)\cos^2(\omega)]\right\}^{-\frac{1}{2}}$$

$$\Delta\Omega_{FF} = \mp\frac{W_e\rho_0}{\sqrt{\mu/a}}\left\{\frac{1+e}{1-e} - 2\frac{W_e\cos(i)\sqrt{1-e^2}}{n} + \frac{W_e^2(1-e)^2}{n^2}[\cos^2(i) + \sin^2(i)\cos^2(\omega)]\right\}^{-\frac{1}{2}} \tag{28}$$

where the sign indicates whether the deputy is ahead of (+) or behind (−) the chief.

C. In-Track/Cross-Track Formations

A formation whose motion is entirely in the in-track/cross-track plane is achieved by requiring the radial position of the deputy to always be zero. Thus, A_1 must be zero in Eq. (13). This is achieved by setting $\Delta e_{ICF} = \Delta M_{ICF} = 0$, and thus, Eq. (13) collapses to

$$x_{ICF} = 0, \qquad y_{ICF} = -A_2\cos(E) + c_1$$

$$z_{ICF} = A_3\sin(E + \psi_3) - c_2 \tag{29}$$

This leaves three design parameters to specify for an in-track/cross-track formation: $\Delta\omega_{ICF}$, Δi_{ICF}, and $\Delta\Omega_{ICF}$.

All in-track/cross-track formations resemble one of two types of motion in the in-track/cross-track plane based on the phase of the cross-track motion, ψ_3. If ψ_3 is equal to 90 deg, then $\beta_2 = 0$, and Eq. (29) describes a straight line with slope s equal to

$$s = \left|\frac{z_a - z_0}{y_a - y_0}\right| = \left|\frac{c_2}{e^2 c_1}\right| \tag{30}$$

The sign of s is determined by z_0. If z_0 is negative, then the deputy is in the bottom half of the in-track/cross-track plane at perigee and s is positive. If z_0 is positive, then the deputy is in the top half of the in-track/cross-track plane at perigee and s is negative.

If ψ_3 is not equal to 90 deg, then Eq. (29) describes an ellipse in the in-track/cross-track plane centered at $[c_1, -c_2]$.

To simplify the following analysis, the chief and deputy are restricted to the linear motion case and, thus, the condition that $\beta_2 = 0$ yields the constraint

$$\cos(\omega)\Delta i_{ICF} + \sin(i)\sin(\omega)\Delta\Omega_{ICF} = 0 \tag{31}$$

The remaining two design parameters characterize the size and shape of the formation at a particular time in the orbit. If the in-track and cross-track separation at perigee are specified, then the remaining two conditions are found from Eq. (29),

$$\cos(i)\Delta\Omega_{ICF} + \Delta\omega_{ICF} = y_0/a(1-e)$$

$$\sin(\omega)\Delta i_{ICF} - \sin(i)\cos(\omega)\Delta\Omega_{ICF} = z_0/a(1-e) \tag{32}$$

Special care must be taken when solving Eqs. (31) and (32) in equatorial ($i = 0$ or 180 deg) and polar ($i = 90$ deg) reference orbits, as well as when perigee of the reference orbit is located at a nodal crossing ($\omega = 0$ or 180 deg). One such case is solved here. If the reference orbit is inclined ($i \neq 0$ or 180 deg) and perigee is located at a nodal crossing ($\omega = 0$ or 180 deg), then Eqs. (31) and (32) are solved by

$$\Delta\Omega_{ICF} = -\frac{z_0}{a(1-e)\sin(i)}$$

$$\Delta\omega_{ICF} = \frac{y_0\sin(i) + z_0\cos(i)}{a(1-e)\sin(i)}, \qquad \Delta i_{ICF} = 0 \tag{33}$$

The maximum and minimum separation between the chief and deputy is determined by first finding an expression for the separation between the chief and deputy as a function of E. If Eqs. (31) and (32) are substituted into Eq. (29), then the separation between the chief and deputy as a function of E for any in-track/cross-track formation is

$$\rho_{ICF} = \sqrt{x_{ICF}^2 + y_{ICF}^2 + z_{ICF}^2} = [1/(1-e)]\Big\{y_0^2[1 - e\cos(E)]^2 + z_0^2[\cos(E) - e]^2\Big\}^{\frac{1}{2}} \tag{34}$$

or, in terms of ν,

$$\rho_{ICF} = [r/a(1-e)]\Big\{y_0^2 + z_0^2\cos^2(\nu)\Big\}^{\frac{1}{2}} \tag{35}$$

The true anomaly at which the extrema of Eq. (35) occur can be found by setting the derivative of Eq. (35) with respect to true anomaly to zero and solving for the values of true anomaly that make the resulting equation true. Thus, the extrema occur at a true anomaly of 0 deg, $\cos^{-1}[e(y_0/z_0)^2]$ deg, and 180 deg. The maximum separation clearly occurs at apogee ($\nu = 180$ deg) and is equal to

$$\rho_{ICF_{max}} = [(1+e)/(1-e)]\rho_0 \tag{36}$$

The minimum separation either occurs at perigee ($\nu = 0$ deg) or $\nu = \cos^{-1}[e(y_0/z_0)^2]$ deg. The ambiguity is resolved by noticing that $\cos^{-1}[e(y_0/z_0)^2]$ only has real solutions when

$$|z_0/y_0| \geq e^{\frac{1}{2}} \tag{37}$$

Thus, if $|z_0/y_0|$ is greater than or equal to $e^{1/2}$, the minimum separation occurs at a true anomaly of the chief of

$$\nu_{ICF_{min}} = \cos^{-1}\left(ey_0^2/z_0^2\right) \tag{38}$$

and is equal to

$$\rho_{\mathrm{ICF}_{\min}} = \left| \frac{y_0 z_0 (e+1)}{\sqrt{e^2 y_0^2 + z_0^2}} \right| \tag{39}$$

If $|z_0/y_0|$ is less than $e^{1/2}$, then the minimum separation between the chief and deputy occurs at perigee and is equal to

$$\rho_{\mathrm{ICF}_{\min}} = \rho_0 \tag{40}$$

Inspection of Eq. (39) reveals an important condition for in-track/cross-track formations: If $y_0 = 0$, then the minimum separation is zero and a collision will occur at $\nu_{\mathrm{ICF}_{\min}}$. Therefore, vehicles in in-track/cross-track formations cannot be aligned in the in-track direction at perigee.

V. Test Formations

For each test formation, the relative motion of a single deputy is examined for a perigee separation of 1 km. Both the chief and deputy are propagated in unperturbed two-body orbits. The true relative positions are determined by propagating the two orbits separately and using Eqs. (7–9) to find the curvilinear coordinates of the deputy. The orbital elements of the deputy are established using the design methods presented in the preceding section. To assess the accuracy of the linearized equations given in Eqs. (10) and (11), these expressions for x, y, z, and their derivatives are compared to the true values. The position error when the chief and deputy are in unperturbed orbits, $P_{2\mathrm{body}}$, is computed by taking the norm of the difference between the unperturbed curvilinear RIC position and Eq. (10),

$$P_{2\mathrm{body}} = \sqrt{(x_{2\mathrm{body}} - x)^2 + (y_{2\mathrm{body}} - y)^2 + (z_{2\mathrm{body}} - z)^2} \tag{41}$$

The velocity error when the chief and deputy are in unperturbed orbits, $V_{2\mathrm{body}}$, is computed by taking the norm of the difference between the unperturbed curvilinear RIC velocity and Eq. (11).

The position and velocity error are a measure of the modeling inaccuracy in Eqs. (10) and (11). It might be tempting to assume that $P_{2\mathrm{body}}$ and $V_{2\mathrm{body}}$ occur independently of one another, but they are coupled. Recall that the derivation of Eqs. (10) and (11) requires the assumption that the orbital elements of the chief and deputy are similar, which implies that the chief and deputy are proximate in position and velocity. Thus, the position and velocity errors are coupled because the validity of Eqs. (10) and (11) is a function of how close the chief and deputy are in position and velocity.

The orbit of the chief for all three test formations is listed in Table 1. The chief appears stationary in each formation because it is always at the origin of the RIC frame.

A. In-Track Test Formation

The deputy only has an in-track component of motion in this formation. For a perigee separation of 1 km and the chief elements given in Table 1, $\Delta\omega_{\mathrm{IF}}$ is 0.00357 deg [Eq. (22)]. All of the other orbital element differences are zero.

Figure 3 shows the in-track position and velocity of the deputy. The radial and cross-track position and velocity are zero within the machine precision. In Fig. 3, the minimum separation between the vehicles is 1 km and the maximum separation is approximately 4.24 km. The predicted minimum and maximum separation [Eqs. (23) and (24)] are within the machine precision of the values in Fig. 3.

The position and velocity errors for the deputy are always zero within the machine precision. This is the result of the simple motion of the deputy and the use of curvilinear coordinates.

B. Follower Test Formation

Both vehicles share the same groundtrack in this formation, with the deputy following the chief. For a perigee separation of 1 km and the chief elements given in Table 1 ΔM_{FF} is -0.00081 deg and $\Delta\Omega_{\mathrm{FF}}$ is 0.00081 deg [Eq. (28)]. The other orbital element differences are zero.

The groundtracks of both vehicles are compared in Fig. 4. The difference between the latitude and longitude of the chief at time t and the latitude and longitude of the deputy at time $t + \Delta M/n$ is

Table 1 Orbital elements of chief in test formations

Parameter	Chief
Perigee radius r_0	16,072 km
Apogee radius r_a	68,120 km
Semimajor axis a	42,096 km
Eccentricity e	0.6182
Inclination i	10 deg
Right ascension of ascending node Ω	0 deg
Argument of perigee ω	0 deg
Mean anomaly at epoch M_0	0 deg

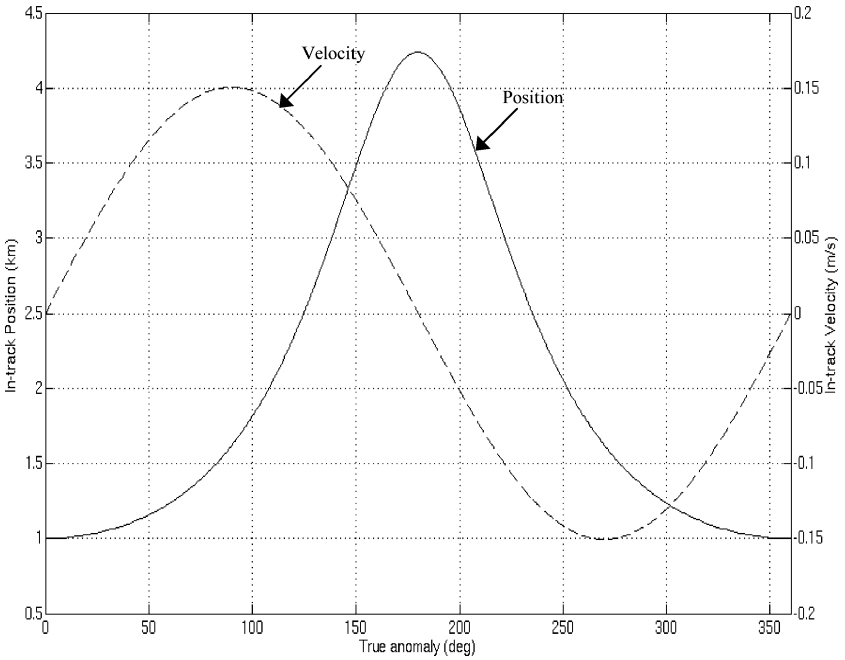

Fig. 3 Curvilinear RIC coordinates for deputy in in-track formation.

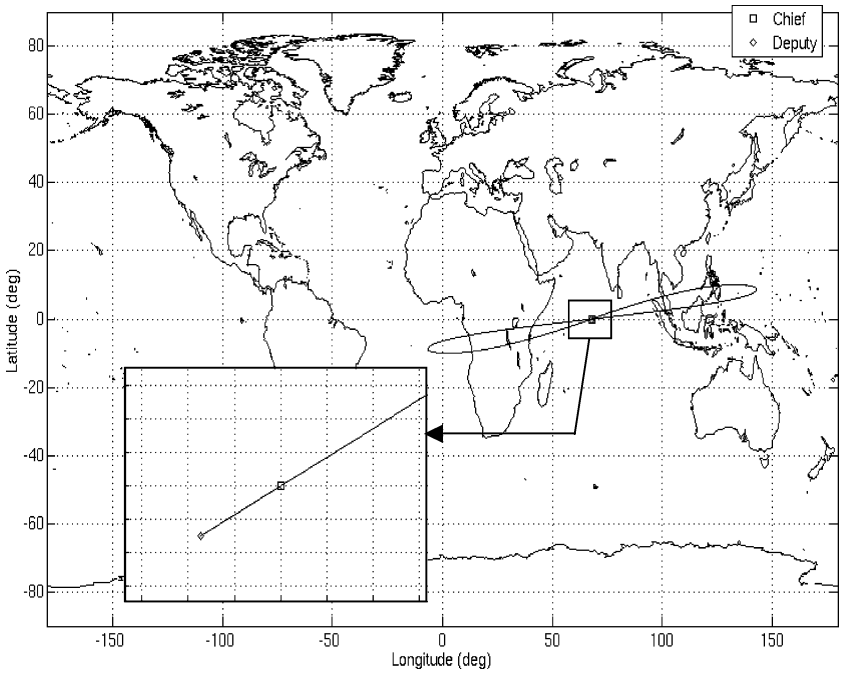

Fig. 4 Groundtrack of chief and deputy in follower formation.

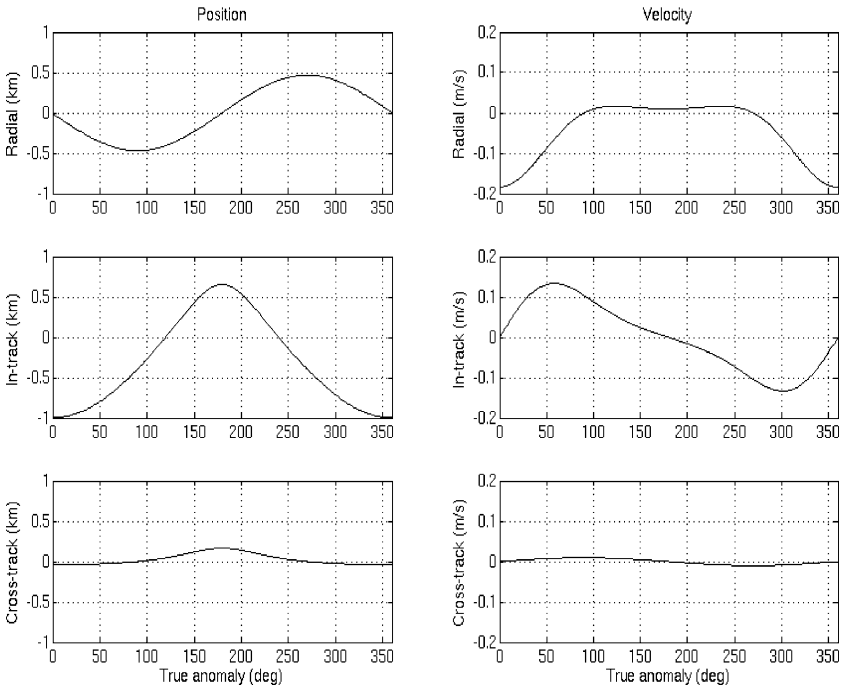

Fig. 5 Curvilinear RIC coordinates for deputy in follower formation.

zero within the machine precision, and thus, the chief and deputy have identical groundtracks (Fig. 4).

Figure 5 shows the radial, in-track, and cross-track position and velocity of the deputy. Most of the motion of the deputy is contained in the radial/in-track plane, with only a slight cross-track motion. This is due to $\sin(i)$ being small in Eq. (26). As $\sin(i)$ increases, so does the magnitude of the cross-track motion.

Figure 6 shows the position and velocity errors for the deputy for five orbital periods. In Fig. 6, both the position and velocity errors are periodic and bounded. The maximum position error is approximately 0.022 m, which is less than 0.006% of the minimum separation of 0.4 km between the vehicles. The maximum velocity error is approximately 0.014 mm/s. In Fig. 7, ρ_0 is varied from 1 to 100 km. The maximum position error in Fig. 7 is not significant for most applications, never exceeding 1% of the minimum separation between the vehicles for a ρ_0 less than 100 km.

C. In-Track/Cross-Track Test Formation

The motion of the deputy in this formation is desired to be linear and contained in the in-track/cross-track plane. Figure 8 shows $\Delta\Omega_{\mathrm{ICF}}$ and $\Delta\omega_{\mathrm{ICF}}$, which were computed using Eq. (33) for $\rho_0 = 1$ km and the values listed in Table 1, as a function of the phase of the deputy at perigee, γ_0. The other orbital element differences are zero.

The evolution of the deputy in the in-track/cross-track plane for several different values of γ_0 is shown in Fig. 9. Figure 10 shows

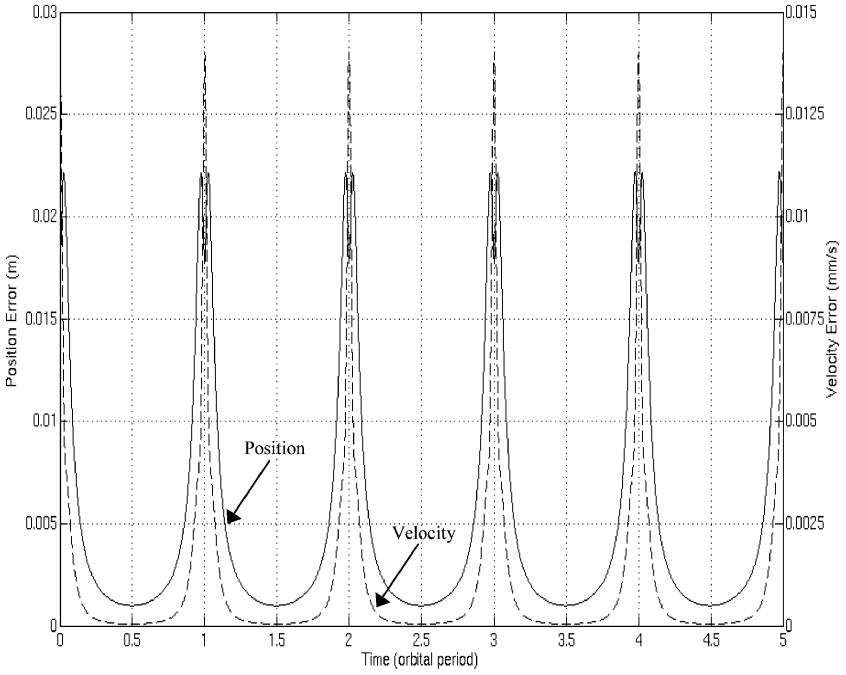

Fig. 6 Two-body position and velocity errors for follower formation.

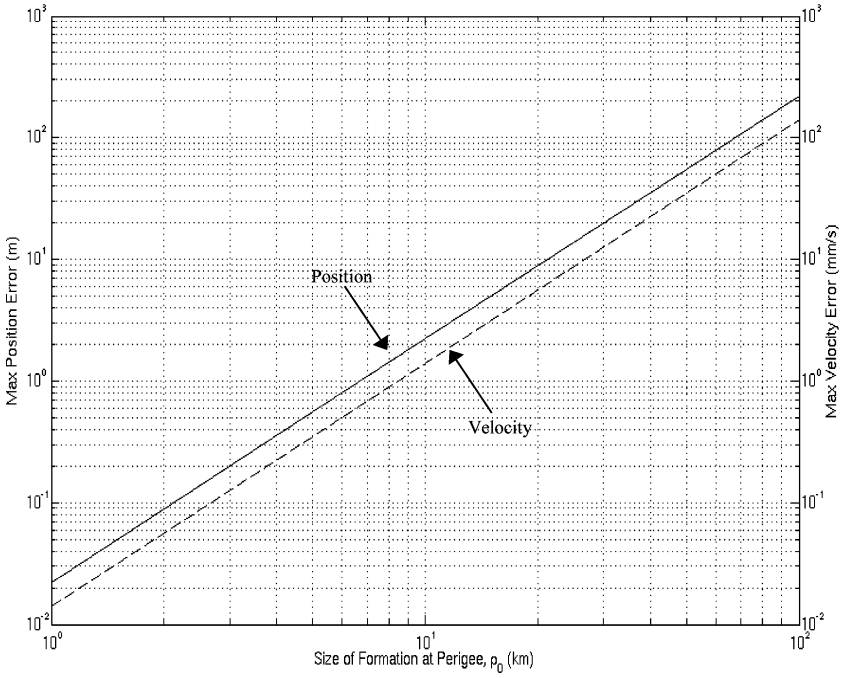

Fig. 7 Maximum two-body errors for follower formation.

the in-track and cross-track position and velocity of the deputy. The radial position and velocity are zero within the machine precision. Figures 9 and 10 show that purely in-track motion results when γ_0 is 0 or 180 deg, that is, when $z_0 = 0$, and purely cross-track motion results when γ_0 is 90 or 270 deg, that is, when $y_0 = 0$. Purely in-track motion was discussed earlier, and the vehicles collide when $y_0 = 0$, so the remainder of this section does not discuss the 0, 90, 180, or 270 deg cases. They shown whenever necessary as envelopes of the relative motion.

Figure 11 shows the separation between the vehicles as a function of γ_0. The maximum separation is independent of γ_0 and is approximately 4.24 km. The maximum separation predicted by Eq. (36) is within the machine precision of the value in Fig. 11. If γ_0 is less than $\tan^{-1}(e^{1/2})$, then the minimum separation in Fig. 11 is approximately 1 km. The minimum separation predicted by Eq. (40) is also within the machine precision of this value. If γ_0 is greater than or equal to $\tan^{-1}(e^{1/2})$, then the true anomaly at which the minimum separation occurs predicted by Eq. (38) and the minimum separation predicted by Eq. (39) are both typically within 0.01% of the values in Fig. 11.

The position and velocity errors for the deputy as a function of several different values of γ_0 are shown in Fig. 12. The interesting result is that deputies with supplementary phases, such as 60 and 120 deg, have different position and velocity errors. At first, this seems inconsistent: The magnitude of the position and velocity for deputies with supplementary phases appears to be the same in

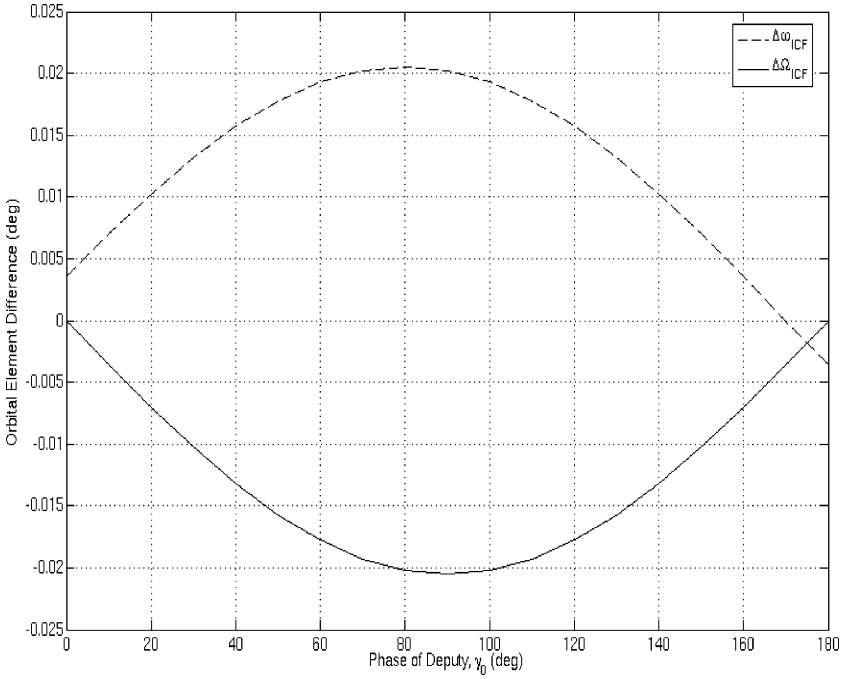

Fig. 8 Orbital element differences for in-track/cross-track formation.

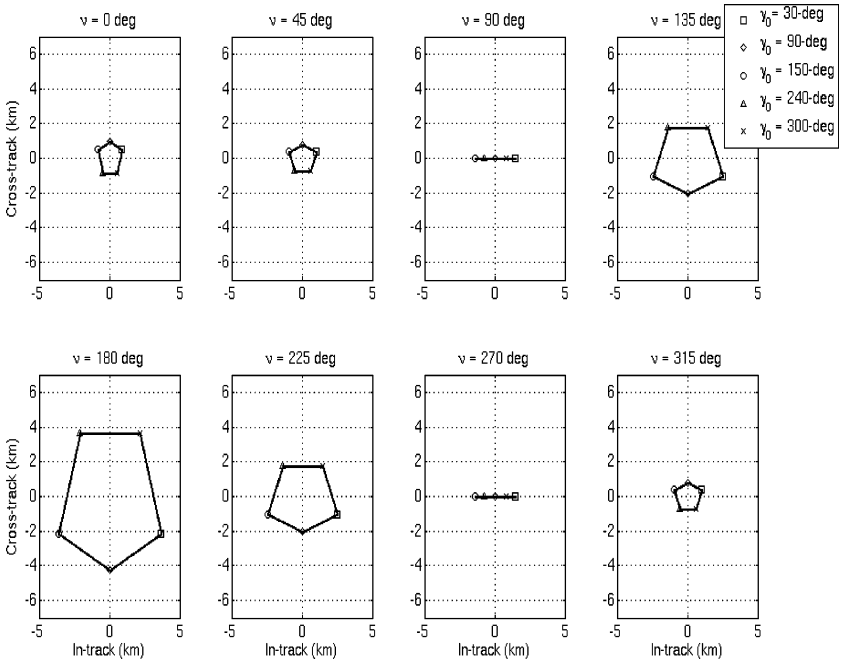

Fig. 9 Evolution of deputy in in-track/cross-track formation.

Fig. 10, and therefore, both deputies should have identical position and velocity errors. However, consider two deputies, one with a phasing of 60 deg (D1) and one with a phasing of 120 deg (D2). Figure 13 shows the cross-track components of the position and velocity errors for D1 and D2. Examination of Figs. 12 and 13 reveals that the cross-track components account for almost all of the position and velocity errors. This is due to a lack of symmetry in the cross-track motion of D1 and D2 that is not captured by Eqs. (10) and (11). When Eqs. (10) and (11) are used the magnitude of the cross-track position and velocity of D1 and D2 are equal at every instant in time. This, however, is not realistic because D1 is ahead of D2 in its orbit. This causes D1 and D2 to have slightly different cross-track positions and velocities at every instant in time. Thus, the position and velocity errors for D1 and D2, and all deputies with supplementary phases, are different. This effect is also present in the in-track direction, but is more noticeable in the cross-track direction because of a greater lack of symmetry between the two orbits in this dimension. The in-track components of the position and velocity error are generally an order of magnitude smaller than the cross-track components.

The position and velocity error is again periodic and bounded in Fig. 12. The maximum position error is always less than 0.35 m, which is approximately 0.05% of the minimum separation between the vehicles. The maximum velocity error is always less than 0.07 mm/s. The size of the formation at perigee is varied from 1 to 100 km in Fig. 14. The maximum position linearization error

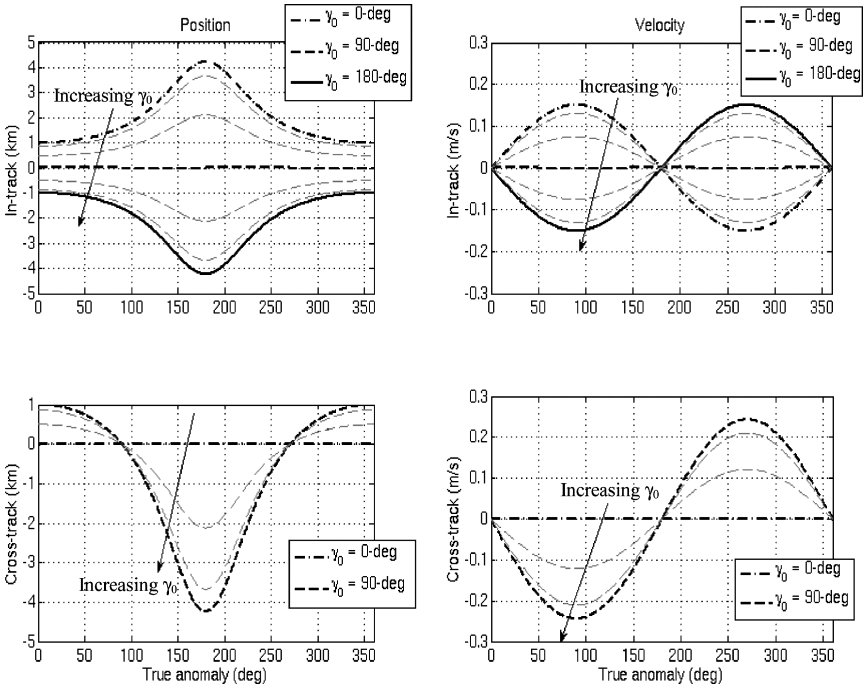

Fig. 10 Curvilinear RIC coordinates for deputy in in-track/cross-track formation.

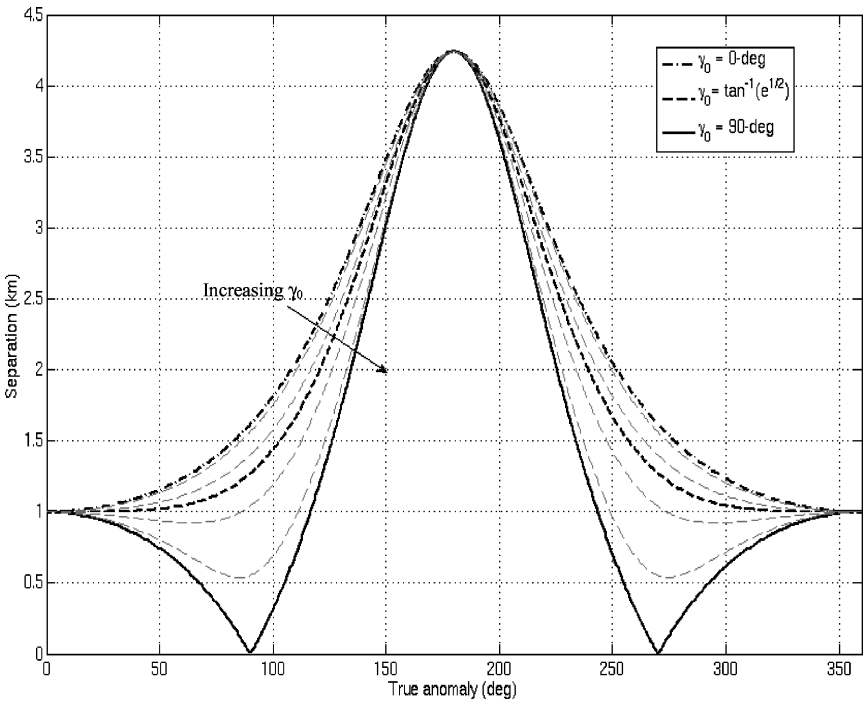

Fig. 11 Vehicle separations for in-track/cross-track formation.

exceeds 1% of the minimum separation at a ρ_0 of approximately 20 km.

VI. Evaluation of Test Formations in Perturbed Orbits

In the preceding section, the accuracy of Eqs. (10) and (11) was examined when the trajectories of the chief and deputy followed unperturbed, two-body orbits. This section evaluates the effects of unmodeled perturbations on the accuracy of Eqs. (10) and (11). Perturbations can cause significant secular drifts in the separation between vehicles that cause the desired formation geometry to degrade over time. How quickly the desired geometry degrades is of practical importance to mission planners because it determines how often formation maintenance maneuvers are required.

The orbits of the chief and deputy for each test formation were propagated in the presence of the perturbation due to J_2, solar radiation pressure (SRP), and the third-body effects of the sun and moon. The models for these perturbations are well known and can be found, for example, in Ref. 19. Table 2 lists the force model parameters used in the propagation of the orbits of the chief and deputy. The perturbation due to atmospheric drag would need to be considered for orbits with perigee altitude less than about 1000 km, but can be safely ignored here (Table 1).

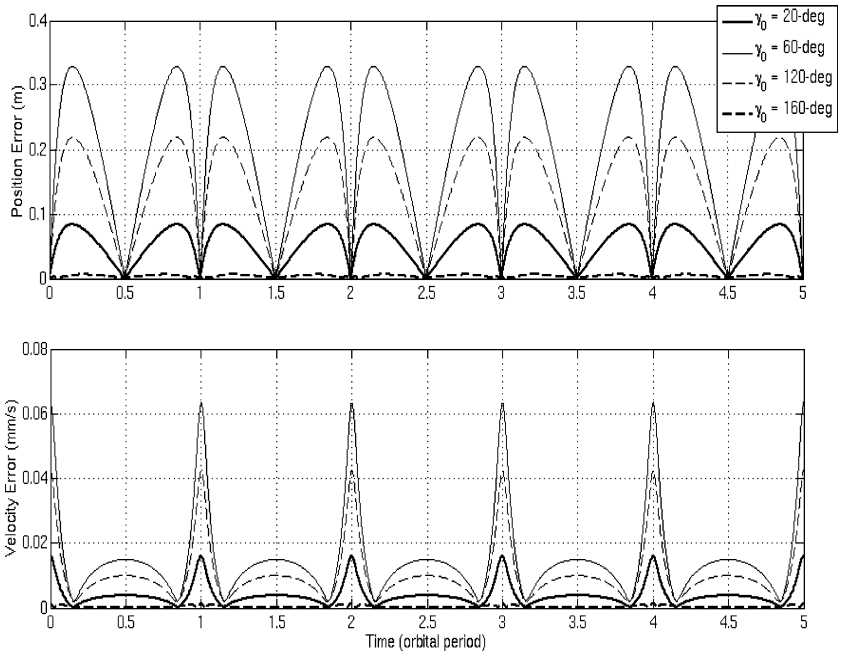

Fig. 12 Two-body position and velocity errors for in-track/cross-track formation.

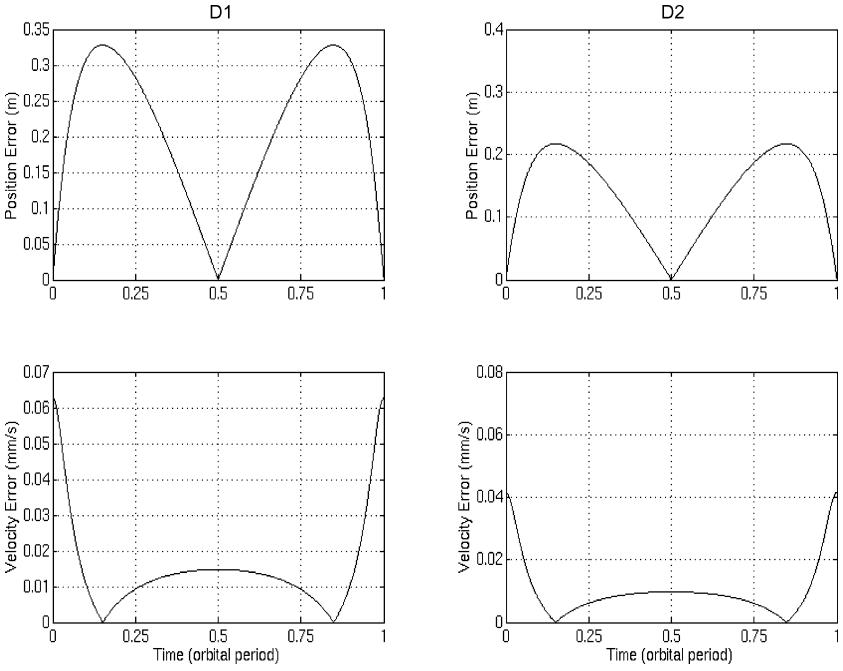

Fig. 13 Cross-track components of two-body position and velocity errors.

Table 2 Force model parameters

Parameter	Value
Start date	8 Nov. 2004 00:00:00
End date	13 Nov. 2004 00:00:00
Integrator	Fourth- and fifth-order variable step Runga–Kutta
Output rate	∼90 s
J_2 value	0.0010826269
Gravitational parameter of sun	1.327124×10^{20} m^3/s^2
Gravitational parameter of moon	4.902799×10^{12} m^3/s^2
Third body	Solar/lunar point masses[a]
SRP	Cylindrical shadow model, $C_r = 1.47$

[a]Based on *Astronomical Almanac* (1992) formula.

The position error when the chief and deputy are in perturbed orbits, P_{pert}, is computed by taking the norm of the difference between the perturbed curvilinear positions and Eq. (10). Similarly, the velocity error V_{pert} is computed by taking the norm of the difference between the perturbed curvilinear velocities and Eq. (11).

Figures 15–17 show the position and velocity error when the chief and deputy are in perturbed orbits for each test formation (in-track, follower, and in-track/cross-track). The errors in Figs. 15–17 are not bounded, although they do show some periodic structure. Table 3 lists in the maximum position and velocity errors for each formation after five orbital periods. (The maximum position and velocity error for the in-track/cross-track formation depends on the phase of the deputy at perigee, and thus, a range of values is shown in Table 3 for this formation.)

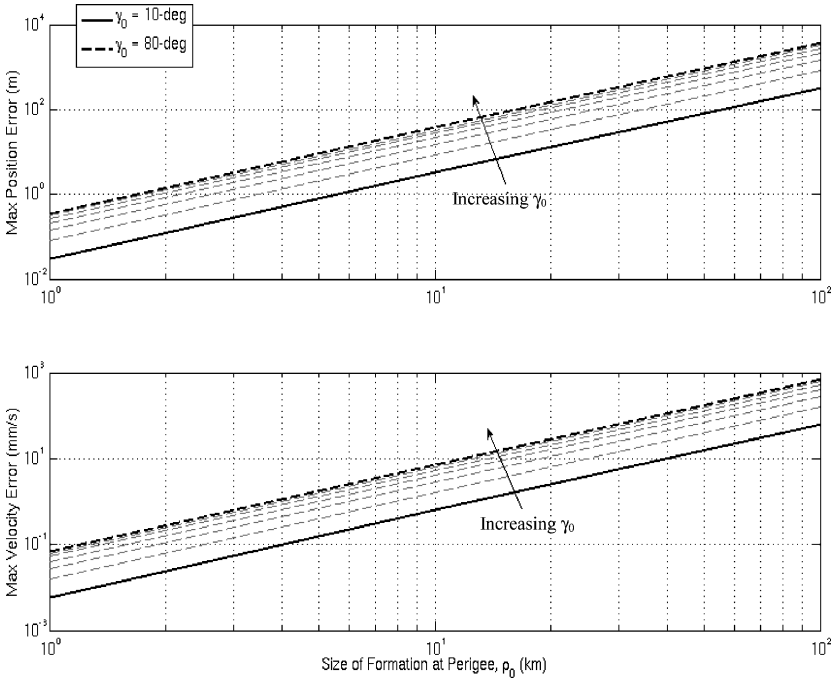

Fig. 14 Maximum two-body errors for in-track/cross-track formation.

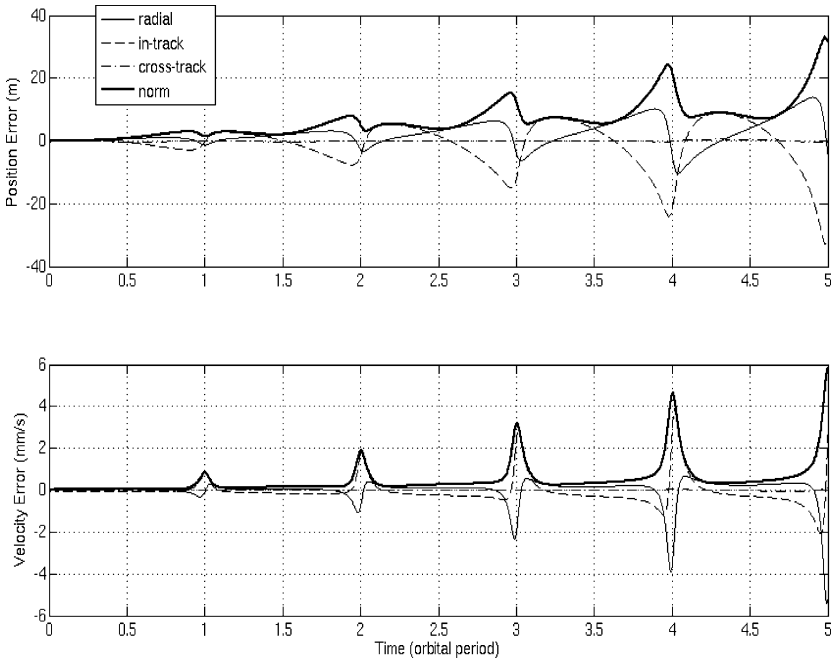

Fig. 15 Perturbed position and velocity errors for in-track formation.

Table 3 Maximum position and velocity errors

Formation type	Maximum position error, m	Maximum velocity error, mm/s
In-track	33	5.9
Follower	7.4	0.58
In-track/cross-track	10–33	1.8–5.9

The secular growth seen in the position and velocity errors in Figs. 15–17 is entirely due to the third-body effects of the sun and moon. The J_2 perturbation causes only periodic position and velocity errors because the constraint $\Delta a = \Delta e = \Delta i = 0$ is imposed in each formation and this forces the nodal, argument of perigee, and mean anomaly drift rates of the chief and deputy due to J_2 to be equal.[19] The maximum position error due to J_2 is less than 2 m for each test formation after five periods. The perturbation due to SRP depends on the particular solar reflectivity and orientation of each vehicle in the formation at each time. The effect is minimized here because it is assumed the solar reflectivity coefficient and orientation of all vehicles in the formation are identical and constant. Whether these assumptions are valid depends on the application. Obviously, if the assumptions are not valid, the effect of SRP will be more pronounced; however in Figs. 15–17, SRP is negligible compared to the effects of the sun and moon.

The third-body effects of the sun and moon induce significant differential drift rates in the node, argument of perigee, and mean anomaly at epoch of the vehicles.[19] The eccentricity and inclination of the chief and deputy also show a slight differential drift rate, but the magnitude of the drift in these orbital elements is far smaller. The secular growth is larger in the radial and in-track components of the position and velocity errors because, for orbits with a high eccentricity and low inclination, the third-body effects of the sun

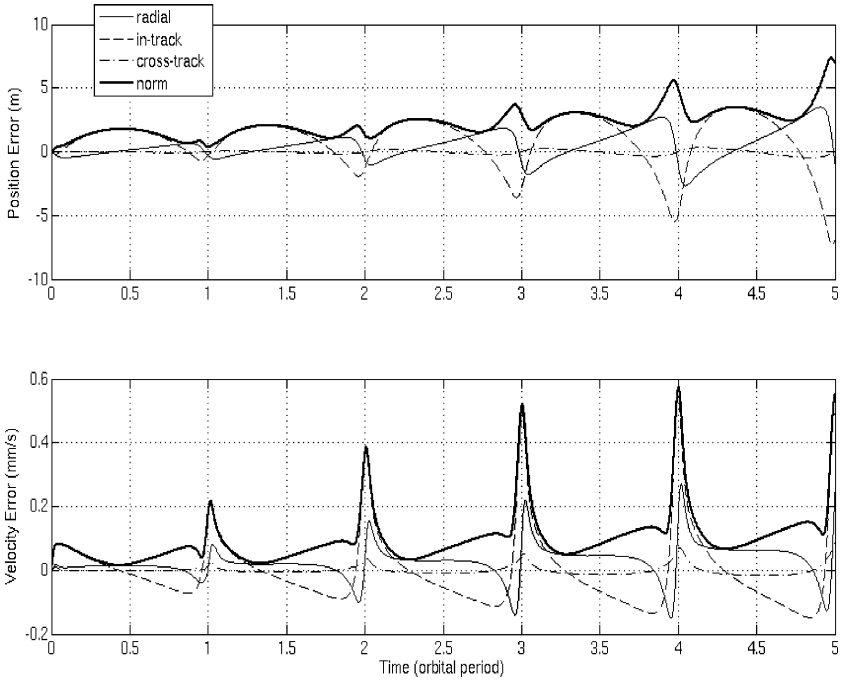

Fig. 16 Perturbed position and velocity errors for follower formation.

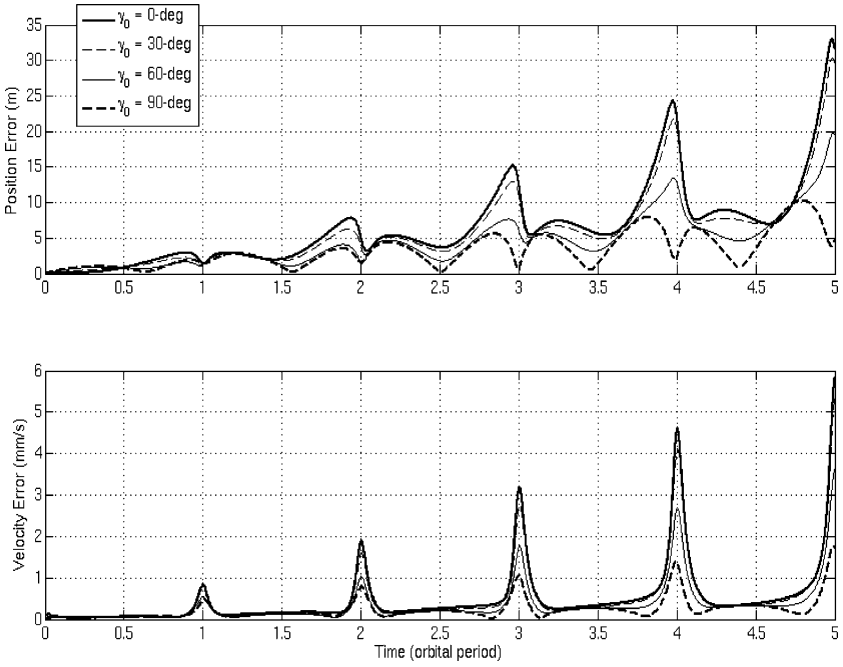

Fig. 17 Perturbed position and velocity errors for in-track/cross-track formation.

and moon have a larger impact on the argument of perigee and mean anomaly than on the node.[19]

VII. Conclusions

A set of geometrical relationships describing the approximate natural relative motion of vehicles in eccentric orbits has been developed to aid in formation design. These expressions extend the availability of intuitive design methods to highly eccentric orbits. Three specific types of passive orbit configurations have been analyzed: 1) an in-track formation, 2) a follower formation, and 3) an in-track/cross-track formation. In each case, the designer selects desired attributes of the formation at perigee (or another reference point in the orbit), and the guidelines provide a means for computing the orbital element differences of each vehicle in the formation. Expressions for minimum and maximum separations are also given to allow these constraints to be considered directly in the design process.

Although perturbations must be considered in the long-term planning of each formation, the geometrical relationships presented are a sufficiently accurate means of modeling the relative motion of one vehicle with respect to another over short intervals, as might be needed, for example, in a relative navigation filter. The fidelity of the linearized model was evaluated by comparisons with true two-body orbit propagation and numerical integration of perturbed orbits. For ideal two-body orbits, the position error was found to be less than 0.35 m and velocity error less than 0.07 mm/s for a 1-km formation at perigee. The perturbations due to the third-body effects of the sun

and moon have been shown to cause a secular drift in the separation between the vehicles that is limited to 33 m after five orbital periods. Other perturbations, such as J_2 and solar radiation pressure, have only a minor impact on the relative motion for the highly elliptical orbits under consideration here.

Whereas it is certain that final design plans for high eccentricity orbit formations will be based on extensive high-fidelity simulations, this work has shown that the usefulness of simplified geometric methods is not limited to near-circular conditions. The extension of the linearized models to the high eccentricity case will facilitate rapid assessment of candidate formations. Other future possibilities are the applications of the formulations given to the design of relative navigation filters and feedback control algorithms.

Appendix: Partial Derivatives

A. Partial Derivatives: r and ν

The partials of r and ν with respect to α are computed by first taking the partials of M with respect to α,

$$M = M_0 + n(t - t_0)$$

$$\Rightarrow \frac{\partial M}{\partial e} = \frac{\partial M}{\partial i} = \frac{\partial M}{\partial \Omega} = \frac{\partial M}{\partial \omega} = 0$$

$$\Rightarrow \frac{\partial M}{\partial a} = -\frac{3n}{2a}(t - t_0), \qquad \frac{\partial M}{\partial M_0} = 1$$

The partials M are then related to the partials of E through Kepler's equation,

$$M = E - e\sin(E)$$

$$\Rightarrow \frac{\partial E}{\partial i} = \frac{\partial E}{\partial \Omega} = \frac{\partial E}{\partial \omega} = 0$$

$$\Rightarrow \frac{\partial E}{\partial a} = \frac{-3n}{2r}(t - t_0), \qquad \frac{\partial E}{\partial e} = \frac{\sin(E)}{1 - e\cos(E)} = \frac{\sin(\nu)}{\sqrt{1 - e^2}}$$

$$\frac{\partial E}{\partial M_0} = \frac{1}{1 - e\cos(E)} = \frac{a}{r}$$

The partials of r can be related to the partials of E through several equations. For example,

$$r = a[1 - e\cos(E)]$$

$$\Rightarrow \frac{\partial r}{\partial i} = \frac{\partial r}{\partial \Omega} = \frac{\partial r}{\partial \omega} = 0$$

$$\Rightarrow \frac{\partial r}{\partial a} = \frac{r}{a} - \frac{3n(t - t_0)e\sin(\nu)}{2\sqrt{1 - e^2}}, \qquad \frac{\partial r}{\partial e} = -a\cos(\nu)$$

$$\frac{\partial r}{\partial M_0} = \frac{ae\sin(\nu)}{\sqrt{1 - e^2}}$$

Similarly, the partials of $\boldsymbol{\nu}$ can be related to the partials of r and E through the equation

$$a\cos(E) = ae + r\cos(\nu)$$

$$\Rightarrow \frac{\partial \nu}{\partial i} = \frac{\partial \nu}{\partial \Omega} = \frac{\partial \nu}{\partial \omega} = 0$$

$$\Rightarrow \frac{\partial \nu}{\partial a} = -\frac{3a}{2r^2}n(t - t_0)\sqrt{1 - e^2}, \qquad \frac{\partial \nu}{\partial e} = \frac{\sin(\nu)}{1 - e^2}[2 + e\cos(\nu)]$$

$$\frac{\partial \nu}{\partial M_0} = \frac{a^2}{r}\sqrt{1 - e^2}$$

B. Partial Derivatives: r

The partial derivatives of $\boldsymbol{r}$ with respect to α are computed using the preceding results for $\partial r/\partial\alpha$ and $\partial\nu/\partial\alpha$:

$$\Rightarrow \frac{\partial \boldsymbol{r}}{\partial a} = \frac{\partial r}{\partial a}\underbrace{\begin{bmatrix} \cos(\Omega)\cos(\theta) - \sin(\Omega)\cos(i)\sin(\theta) \\ \sin(\Omega)\cos(\theta) - \cos(\Omega)\cos(i)\sin(\theta) \\ \sin(i)\sin(\theta) \end{bmatrix}}_{\Lambda_1}$$

$$+ r\frac{\partial \nu}{\partial a}\underbrace{\begin{bmatrix} -\cos(\Omega)\sin(\theta) - \sin(\Omega)\cos(i)\cos(\theta) \\ -\sin(\Omega)\sin(\theta) + \cos(\Omega)\cos(i)\cos(\theta) \\ \sin(i)\cos(\theta) \end{bmatrix}}_{\Lambda_2}$$

$$\Rightarrow \frac{\partial \boldsymbol{r}}{\partial e} = \frac{\partial r}{\partial e}\Lambda_1 + r\frac{\partial \nu}{\partial e}\Lambda_2, \qquad \frac{\partial \boldsymbol{r}}{\partial M_0} = \frac{\partial r}{\partial M_0}\Lambda_1 + r\frac{\partial \nu}{\partial M_0}\Lambda_2$$

$$\Rightarrow \frac{\partial \boldsymbol{r}}{\partial i} = r\begin{bmatrix} \sin(\Omega)\sin(i)\sin(\theta) \\ -\cos(\Omega)\sin(i)\sin(\theta) \\ \cos(i)\sin(\theta) \end{bmatrix}$$

$$\frac{\partial \boldsymbol{r}}{\partial \Omega} = r\begin{bmatrix} -\sin(\Omega)\cos(\theta) - \cos(\Omega)\cos(i)\sin(\theta) \\ \cos(\Omega)\cos(\theta) - \sin(\Omega)\cos(i)\sin(\theta) \\ 0 \end{bmatrix}$$

$$\Rightarrow \frac{\partial \boldsymbol{r}}{\partial \omega} = r\begin{bmatrix} -\cos(\Omega)\sin(\theta) - \sin(\Omega)\cos(i)\cos(\theta) \\ -\sin(\Omega)\sin(\theta) + \cos(\Omega)\cos(i)\cos(\theta) \\ \sin(i)\cos(\theta) \end{bmatrix}$$

Thus, the partials of $\boldsymbol{r}$ with respect to α can be written as the sensitivity matrix S_{ECI},

$$S_{\mathrm{ECI}} = \left[\frac{\partial \boldsymbol{r}}{\partial a}\middle|\frac{\partial \boldsymbol{r}}{\partial e}\middle|\frac{\partial \boldsymbol{r}}{\partial i}\middle|\frac{\partial \boldsymbol{r}}{\partial \Omega}\middle|\frac{\partial \boldsymbol{r}}{\partial \omega}\middle|\frac{\partial \boldsymbol{r}}{\partial M}\right]_{3\times 6}$$

Acknowledgments

This work was funded under Cooperative Agreement NCC5-721 through the NASA Goddard Space Flight Center Formation Flying NASA Research Announcement. Any opinions, findings, and conclusions or recommendations expressed in this material are those of the authors and do not necessarily reflect the views of the National Aeronautics and Space Administration. The authors thank Michael Moreau, Russell Carpenter, and Steven Hughes of NASA Goddard Space Flight Center, as well as the Associate Editor and anonymous reviewers, for their insights and suggestions.

References

[1]Ticker, R. L., and McLennan, D., "The New Millennium Program Space Technology 5 (ST5)," *Proceedings of Space 2000: The 7th International Conference and Exposition on Engineering, Construction, Operations, and Business in Space*, American Society of Civil Engineers, Reston, VA, 2000, pp. 469–475.

[2]Carpenter, K. G., Schrijver, C. J., Lyon, R. G., Mundy, L. G., Allen, R. J., Armstrong, J. T., Danchi, W. C., Karovska, M., Marzouk, J., Mazzuca, L. M., Mozurkewich, D., Neff, S. G., Pauls, T. A., Rajagopal, J. K., Solyar, G., and Zhang, X., "Stellar Image (SI) Mission Concept," *Proceedings of the Society of Photo-Optical Instrumentation Engineers*, edited by J. C. Blades and O. H. Siegmund, Vol. 4854, Society of Photo-Optical Instrumentation Engineers, Bellingham, WA, 2003, pp. 293–302.

[3]NASA Announcement of Opportunity, "Terrestial Planet Finder (TPF)," No. NRA-03-OSS-01-TPF, URL: http://research.hq.nasa.gov/code_s/nra/current/AO-03-OSS-01/index.html [cited 3 March 2003].

[4]NASA Announcement of Opportunity, "Magnetospheric Multiscale Mission (MMS)," No. AO-03-OSS-01, URL: http://research.hq.nasa.gov/code_s/dynamic.cfm?op_fy=2003 [cited 3 Jan. 2003].

[5]Fridlund, M., and Gondoin, P., "The Darwin Mission," *Interferometry in Space*, Society of Photo-Optical Instrumentation Engineers, Bellingham, WA, pp. 394–404.

[6]Lawden, D. F., *Journal of the British Interplanetary Society*, Vol. 13, No. 2, 1954, pp. 87–101.

[7]Tschauner, J., and Hempel, P., "Optimale Beschleunigungs-propgramme fur des rendezvous Manover," *Astronautica Acta*, Vol. 10, Nos. 5–6, 1964, pp. 296–307.

[8]Carter, T. E., "New Form for the Optimal Rendezvous Equations Near a Keplerian Orbit," *Journal of Guidance, Control, and Dynamics*, Vol. 13, No. 1, 1990, pp. 183–186.

[9]Garrison, J. L., Gardner, T. G., and Axelrad, P., "Relative Motion in Highly Elliptical Orbits," *Proceedings of the 5th AAS/AIAA Spaceflight Mechanics Conference*, edited by R. J. Proulx, J. J. F. Liu, P. K. Seidelmann, and S. Alfano, Vol. 89, American Astronautical Society, San Diego, CA, 1995, pp. 1359–1376.

[10]Gim, D. W., and Alfriend, K. T., "State Transition Matrix of Relative Motion for the Perturbed Noncircular Reference Orbit," *Journal of Guidance, Control, and Dynamics*, Vol. 26, No. 6, 2003, pp. 956–971.

[11]Sabol, C., McLaughlin, C. A., and Luu, K. K., "Meet the Cluster Orbits with Perturbations of Keplerian Elements (COWPOKE) Equations," *Advances in the Astronautical Sciences*, Vol. 114, Pt. 1, 2003, pp. 573–594.

[12]Melton, R. G., "Time-Explicit Representation of Relative Motion Between Elliptical Orbits," *Journal of Guidance, Control, and Dynamics*, Vol. 23, No. 4, 2000, pp. 604–610.

[13]Sabol, C., Burns, R., and McLaughlin, C. A., "Satellite Formation Flying Design and Evolution," *Journal of Spacecraft and Rockets*, Vol. 38, No. 2, 2001, pp. 270–278.

[14]Lovell, T. A., and Tragesser, S. G., "Analysis of the Reconfiguration and Maintenance of Close Spacecraft Formations," *Spaceflight Mechanics 2003*, Vol. 1, San Diego, CA, 2003, pp. 595–609.

[15]Hill, G. W., "Researches in the Lunar Theory," *American Journal of Mathematics*, Vol. 1, 1878, pp. 5–26, 129–147, 245–260.

[16]Inalhan, G., Tillerson, M., and How, J. P., "Relative Dynamics and Control of Spacecraft Formations in Eccentric Orbits," *Journal of Guidance, Control, and Dynamics*, Vol. 25, No. 1, 2002, pp. 48–59.

[17]Broucke, R. A., "Solution of the Elliptic Rendezvous Problem with the Time as Independent Variable," *Journal of Guidance, Control, and Dynamics*, Vol. 26, No. 4, 2003, pp. 615–621.

[18]Battin, R. H., *An Introduction to the Mathematics and Methods of Astrodynamics*, AIAA Education Series, AIAA, New York, 1987, Chap. 3.

[19]Vallado, D. A., *Fundamentals of Astrodynamics and Applications*, 2nd ed., Microcosm Press, El Segundo, CA, 2001, Chaps. 3, 5, 6, 8, 9.

[20]Schaub, H., and Alfriend, K. T., "$J2$ Invariant Relative Orbits for Spacecraft Formations," *Celestial Mechanics and Dynamical Astronomy*, Vol. 79, No. 2, 2001, pp. 77–95.